Title

Near-Infrared and Visible Photoactivation to Uncage Carbon Monoxide from an Aqueous-Soluble PhotoCORM

Journal

Inorganic Chemistry, 58(16)

ISSN

0020-1669

Authors

Jiang, Qin
Xia, Yingzi
Barrett, Jacob
et al.

Publication Date

2019-08-19

DOI

10.1021/acs.inorgchem.9b01581

Near-Infrared and Visible Photoactivation to Uncage Carbon Monoxide from an Aqueous-Soluble PhotoCORM.

Qin Jiang,[a,b,*] Yingzi Xia,[a] Jacob Barrett,[a] Alexander Mikhailovsky,[a] Guang Wu,[a] Daqi Wang,[c] Pengfei Shi [b,*] and Peter C. Ford[a,*]

[a] Department of Chemistry and Biochemistry, University of California, Santa Barbara, Santa Barbara, CA, 93106 USA

[b] School of Chemistry and Chemical Engineering, Jiangsu Ocean University, Lianyuangang 222005, Jiangsu, PR China

[c] School of Chemistry and Chemical Engineering, Liaocheng University, Liaocheng 252000, Shandong, PR China

KEYWORDS: Two-photon excitation, photoCORM, manganese carbonyl, carbon monoxide release

ABSTRACT: Multiphoton excitation allows one to access high energy excited states and perform valuable tasks in biological systems using tissue penetrating near-infrared (NIR) light. Here we describe a new photoactive manganese tricarbonyl complexes incorporating the ligand 4'-p-N,N-bis(2-hydroxyethyl)benzyl-2,2':6',2''-terpyridine (TPYOH), which can serve as an antenna for two photon NIR excitation. Solutions of $Mn(CO)_3(TPYOH)X$ (X = Br^- or $CF_3SO_3^-$) complexes are very photoactive towards CO release under visible light excitation (405 nm, 451 nm). The same responses were also triggered by multiphoton excitation at 750 nm and 800 nm. In this context, we discuss the potential applications of these complexes as visible/near-IR light photoactivated carbon monoxide releasing moieties (photoCORMs). We also report the isolation and crystal structures of the TPYOH complexes $Mn(TPYOH)Cl_2$ and $[Mn(TPYOH)_2](CF_3SO_3)_2$, to illustrate possible photolysis product(s).

INTRODUCTION

The discoveries that carbon monoxide plays important roles in mammalian physiology has changed the perception of CO from simply being a toxin to something with much broader biological implications.[1-3] These roles include cytoprotection, vasoactive response, modulation of the immune system and redox control.[4] Low doses of CO are anti-inflammatory, and have potential therapeutic applications in wound healing and in reducing organ graft rejection.[5-8] However, therapeutic application of CO gas faces serious obstacles owing to toxicity and lack of tissue specificity.[9] Compounds that release CO in a controllable manner have thus drawn interest as potential therapeutic drugs. Endogenous and exogenous triggers have been studied, including ligand exchange, enzymatic reactions and photolabilization.[5] Photoactivated CO-releasing moieties (photoCORMs)[10] have advantages such as stability in dark, controllability of timing, dosage and location of delivery and in some cases visualization of such delivery.[11-13] However, one limitation is that most photoCORMs require UV or shorter visible wavelength light to trigger CO release. These wavelengths do not penetrate tissue deeply and may have detrimental effects on biological targets. Thus, various researchers have employed molecular engineering to shift photoCORM lability to longer wavelengths.[14-20]

The "phototherapeutic window" of mammalian tissues is ~750 to 1100 nm in the near infrared (NIR) wavelength region.[21] For this reason there has been considerable interest in developing multi-photon strategies for uncaging small molecule bioregulators, such as NO or CO, with such excitation wavelengths. Multiphoton excitation allows one to access reactive high energy excited states and to perform valuable tasks in biological systems while using tissue penetrating NIR light.[22-24] In one approach to this goal, our UCSB laboratory and others have utilized NIR to visible up-converting nanoparticles (UCNPs) as antennas and templates to achieve NO[25] or CO[26,27] release from various nanocarriers using sequential absorption of multiple NIR photons.

An alternative approach is the simultaneous two-photon excitation (TPE) of an antenna to sensitize photoactivated uncaging with high intensity NIR light. For examples, Wecksler et al[28,29] and Zheng et al[30] demonstrated TPE initiated NO release from derivatives of Roussin's red salt ester ($Fe_2(\mu\text{-}RS)_2(NO)_4$, R being a chromophore with a high TPE cross-section) using ultrafast 800 nm pulses from a Ti:sapphire laser. This approach has subsequently been exploited by others for similar uncaging.[31,32]

Similar NIR TPE activation of a photoCORM would allow for precise external control of CO delivery to desired targets.

In this context, we report here the design and photochemistry of a new photoCORM that can be activated by TPE with 800 nm light. The TPE antenna is the terpyridine (tpy) derivative, 4'-p-N,N-bis(2-hydroxy-ethyl)-benzyl-2,2':6',2''-terpyridine (TPYOH).[33,34] The TPYOH chromophore has an A-π-A' configuration comprised of an aniline with two hydroxyethyl groups acting as an acceptor (A), a phenyl π-bridge, and a tpy acting as another acceptor (A') and has been shown by our JOU laboratory to have a moderate two-photon absorption cross-sections.[33] The hydroxyethyl groups also enhance aqueous solubility. The tpy functionality serves as the attachment site to a manganese(I) carbonyl fragment, and this combination elicits two-photon activated CO release with NIR. Notably, during the preparation of these results for publication, another laboratory independently reported the generation of CO via the TPE of a manganese carbonyl complex.[35]

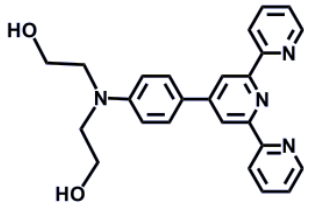

TPYOH

RESULTS AND DISCUSSION

Synthesis and characterization

The general synthesis of the complexes $Mn(CO)_3(\eta^2$-TPYOH)X, X = Br^- (**1**) or $CF_3SO_3^-$ (**2**), is presented in Scheme 1. Complex **1** was purified by chromatography on a neutral alumina column with ethyl acetate /methanol (v:v 1:1) as eluent. Analytical and spectroscopic data confirmed the successful synthesis and purity of two complexes.

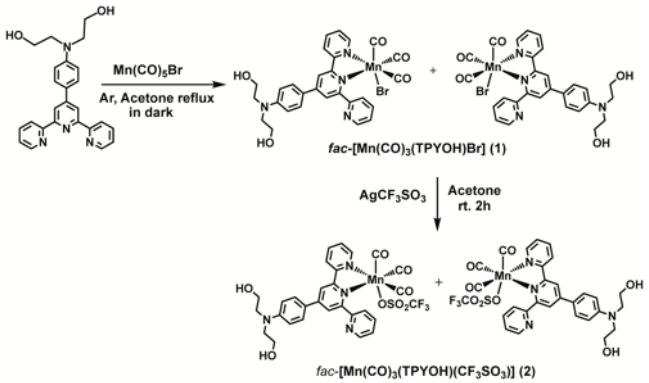

Scheme 1. Synthesis scheme for complexes **1** and **2.**

The solid-state X-ray crystal structure of $Mn(CO)_3$(TPYOH)Br shows three facially coordinated carbonyl ligands and bidentate TPYOH coordinated via the center pyridyl N(1) and one pendant pyridyl (N(2), Fig. 1). The Mn–N(1) bond (2.008(5) Å) is shorter than the Mn–N(2) bond (2.087(5) Å, while the uncoordinated pyridyl nitrogen, N(3), is positioned on the same side as the bromide, with a Mn-N(3) distance of 4.241(5) Å.), as seen with previously reported Mn(I) terpyridine complexes.[33] The structure is chiral and the two *fac*-enantiomers appear in the unit cell (centrosymmetric space group *P-1*) making the overall mixture racemic (Supporting Information(SI) Fig. S1). Other structure details are listed in SI Tables S1 and S2.

The ATR infrared spectra of complexes **1** and **2** display the familiar patterns of the *fac*-$M(CO)_3$ arrangement with ν_{CO} bands at 2017, 1937 and 1885 cm^{-1} for **1**, and at 2033 cm^{-1} and a broad band at 1923 cm^{-1} for **2**, respectively (SI Fig. S2). Complex **2** also shows strong ν_{SO3} bands at 1276 and 1029 cm^{-1} and ν_{CF3} bands at 1164 and 1247 cm^{-1}.

The ^{1}H NMR spectra of TPYOH and of **1** and **2** (SI Figs. S3 and S4, respectively) demonstrate the purity of these samples. In the aromatic region (Fig. 2), all twelve protons expected for bidentate coordination of TPYOH are assignable while the more symmetrical free ligand shows seven proton resonances. Replacement of the bromide of **1** by triflate to give **2** leads to a downfield shift of all the aromatic proton resonances with the maximum $\Delta\delta$ of 0.16 ppm (SI Table S3).

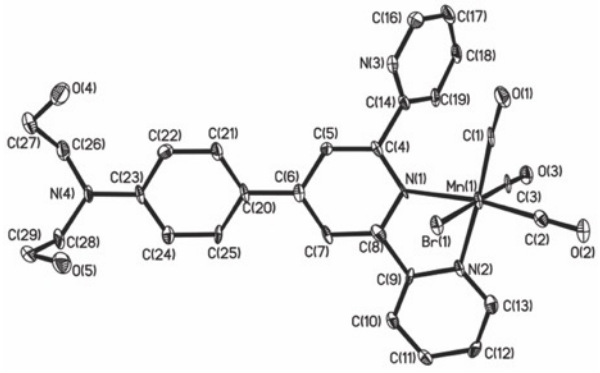

Figure 1. Crystal structure of complex **1**.

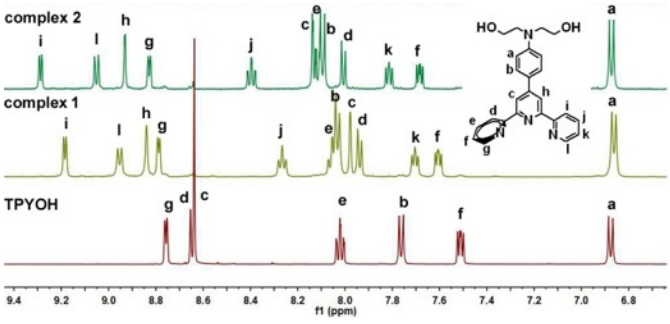

Figure 2. Aromatic region of the ^{1}H NMR spectra of complexes **1** and **2** and of TPYOH in DMSO-d_6.

The ESI-MS^+ spectra for complexes **1** and **2** in CH_3OH/CH_3CN solution display peaks at m/z = 551.1 and 592.1, corresponding to the cations $[Mn(CO)_3(TPYOH)]^+$ and $[Mn(CO)_3(TPYOH)(CH_3CN)]^+$, respectively (SI Fig. S5),

thereby confirming that the $Mn(CO)_3$(TPYOH) unit remains intact.

The triflate complex **2** is moderately soluble in water while the bromide complex **1** is soluble in the mixed ethanol/water (v:v 2:1) solution. The absorption spectra of **1** and **2** in several different solvents are displayed in SI Figure S6 and in other figures below and summarized in Table 1. The visible spectra are dominated by surprisingly strong metal-to-ligand (Mn(I)→TPYOH) charge transfer (MLCT) bands while the UV spectra are dominated by very strong π–π* intra-ligand (IL) bands characteristic of TPYOH. The same MLCT λ_{max} value (428 nm) was observed for the two complexes in ethanol-water but the extinction coefficients were different. For **2**, the MLCT band λ_{max} red shifts ~20 nm when the solvent is changed from water (415 nm) to ethanol (435 nm). The UV-vis spectrum of **2** showed only very minor (≤1%) changes in the MLCT absorbance over a 24 h period in aerobic aqueous solution at 37 °C (SI Fig. S7), indicating its likely stability under biological conditions.

Table 1. UV/Vis absorption bands λ_{max} in nm (ε in M^{-1} cm^{-1}) for TPYOH, $Mn(CO)_3(\eta^2$-TPYOH)Br (**1**) and $Mn(CO)_3(\eta^2$-TPYOH)(CF_3SO_3) (**2**) in water, ethanol and ethanol-water (v:v 2:1).

Complex	UV-vis, λ ($\varepsilon \times 10^4$)
1[a]	428 (3.53), 311 (2.98), 267 (2.79), 208 (5.86)
2[a]	428(2.86), 309 (2.43), 268 (2.27), 209 (4.95)
2[b]	435 (2.41), 311 (1.98), 268 (1.90), 209 (3.71)
2[c]	415 (1.92), 307 (1.79), 200 (4.01)
TYPOH[a]	351 (2.56), 289 (2.87), 234 (2.80), 205 (2.90)

[a] ethanol-water (v:v 2:1). [b] ethanol. [c] water

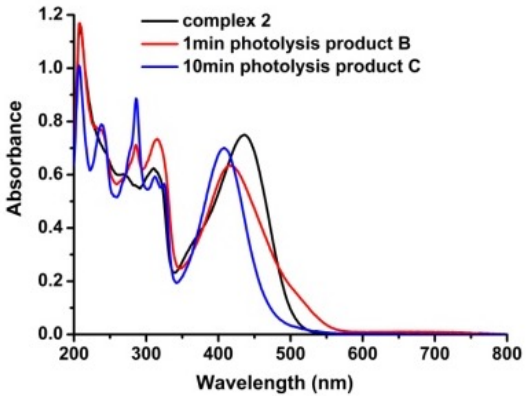

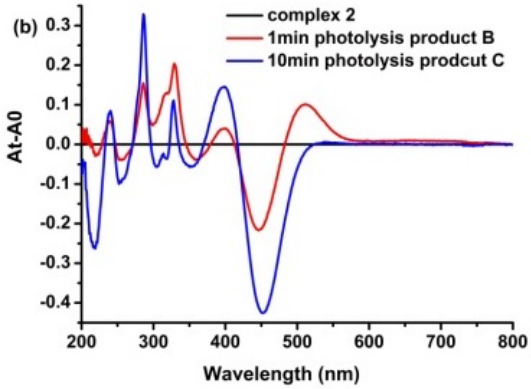

Figure 3. *Top:* Absorption spectra changes upon 451 nm (2.2 mW) photolysis of complex **2** (31 μM) in aerobic ethanol *Bottom*: Difference spectra for same experiment.

Single photon uncaging of CO

Initial photolysis experiments mainly focused on the triflate complex **2**. The excitation sources were light-emitting diodes (LEDs) operating at 451 nm (royal blue) and at 405 nm (The LED emission spectra are shown in SI Figure S8). Figure 3 illustrates the spectral changes when an aerobic ethanol solution of complex **2** (~31 μM) in a quartz Schlenk cuvette was irradiated with the 451 nm LED (2.2 mW). The reaction occurs in two stages. There were rapid initial spectral changes over the first 60 s to give a species (**B**), which displays a MLCT band at ~420 nm but is most prominently indicated in the difference spectrum by a new absorbance at ~524 nm. This is followed by slower changes over the next few (~10) minutes of photolysis indicating the formation of a second species (**C**) with a strong absorption band at 408 nm and no longer showing the 524 nm absorbance in the difference spectra (Fig. 3). SI Figure S9 shows the temporal spectral changes noted over the first 600 s of photolysis in aerobic ethanol. Further exhaustive photolysis (50 min) showed very little spectral change (SI Fig. S10) under these conditions. Similar spectral changes were observed for the photolysis of 2 in aerobic aqueous solution (SI Fig. S11).

Figure 4 plots the relative absorbances $(A_t–A_0)/A_0$ at the MLCT λ_{max} (435 nm) vs photolysis time for the 451 nm irradiation (2.8 mW) of complex **2** in anaerobic and aerobic ethanol. For the first stage (Fig. 4 top), both solutions show a rapid photo-induced decrease, but there is little or no difference in the rate of the process between the aerobic or anaerobic solutions. Figure 4 bottom depicts the second stage by comparing the temporal absorbance changes at 524 nm after an initial 451 nm excitation for 60 s (i.e., after the first stage). In the dark, the anaerobic solution changes little (<4%), but this absorbance decreases ~40% over a period of 60 min in aerobic media. Under continued photolysis at 451 nm, the 524 nm band characteristic of species **B** decreases rapidly in both aerobic and anaerobic EtOH solutions, the rate being somewhat faster in aerobic media.

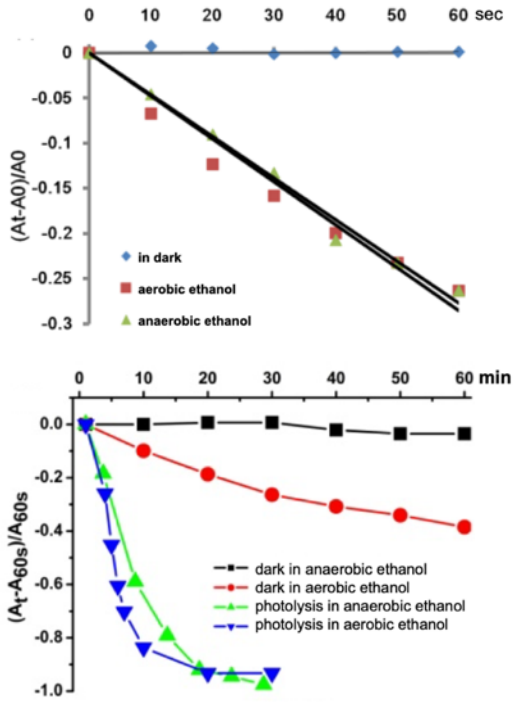

Figure 4. *Top*: Absorbance changes at 435 nm during the first 60 s irradiation (451 nm, 2.8 mW) and in the dark of fresh solutions of **2** in aerobic (32 μM) and anaerobic (36 μM) ethanol. *Bottom:* Absorbance changes at 524 nm during the subsequent 60 min under continued irradiation and in the dark after initial 60 s photolysis.

The two-stage photolysis reaction is also observed in the ν_{CO} region of the infrared spectra. Photolysis of an aerobic ethanol solution of **2** (20 mM) in a 0.1 mm pathlength infrared cell with 451 nm light (2.0 mW) led to decreases in the ν_{CO} bands characteristic of the starting complex and initial appearance of ν_{CO} peaks at 2060, 1975 and 1867 cm^{-1} (Fig. 5). Although we did not study kinetics related to these bands in detail, the appearance and subsequent disappearance of the first two bands upon continued photolysis appeared coupled while the band at 1867 cm^{-1} was more persistent suggesting that it may represent a third species. All three bands also slowly disappeared without continued photolysis, consistent with the dark reaction noted for aerobic solutions of **B** in Figure 4 (bottom).

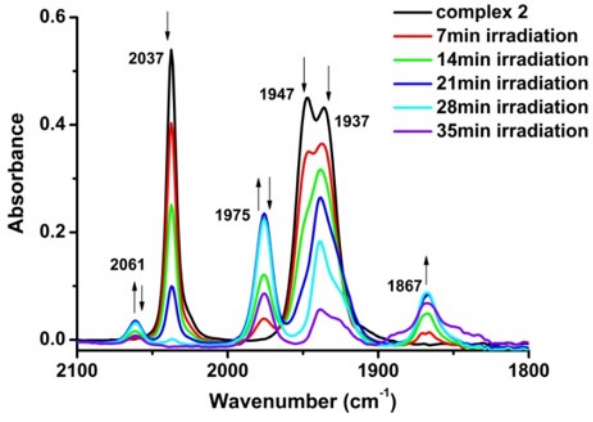

Figure 5. IR spectral changes upon 451 nm (2.1 mW) photolysis of **2** (20 mM) at 7 min intervals for 35 min in aerobic ethanol in a 0.1 cm pathlength KBr cell .

Photodissociation of CO was confirmed by analysis of the gas phase above such solutions using quantitative gas chromatography with thermal conductivity detection (GC-TCD). An aerobic ethanol solution of **2** (2.9 x 10^{-5} M) in a Schlenk cuvette[10] was photolyzed for 60 s with the 451 nm LED giving largely product B according to the absorption spectra changes. GC-TCD analysis of the gas phase above the solution indicated that 0.9 ± 0.2 moles of CO were released per mole of **2** present (SI Table S4). Further, more exhaustive, photolysis (~30 min) led to the release of ~two more CO's upon formation of **C**. No CO_2 above background levels was found as a product of either of these photochemical stages.

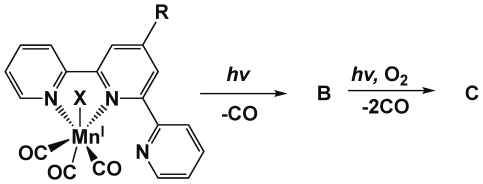

Scheme 2. Proposed photoreaction pathway for the Mn(I) complex **2** (R is N,N-bis(2-hydroxyethyl)benzyl, X is triflate or solvent).

This pattern suggests a reaction sequence such as Scheme 2, where the first step is CO photo-dissociation from **2** to give a dicarbonyl complex **B**. It is unclear whether the TPYOH ligand in **B** is tricoordinate, although similar sequence reported by Compain et al for photolysis of acetonitrile solutions of related η^2-terpyridine complexes gave the related analogous tricoordinate η^3-terpyridine species.[36] Given that the second, slower photoreaction stage **B** → **C** occurs in anaerobic media but appears to be accelerated by the presence of oxygen, this may lead to several products.

DFT calculations at the B3LYP/6-31G* level were used to gain insight into the electronic spectra of the η^2-TPYOH complex **1** and of the tridentate analogue $Mn(CO)_2(\eta^3\text{-TPYOH})Br$. The HOMOs of the optimized ground state structures for both complexes are mainly localized on the Mn center, while the LUMOs have considerable contributions from two and three pyridines, respectively (SI Fig. S12). Thus, the HOMO → LUMO transitions for both complexes can be assigned as metal to ligand charge transfer (MLCT) transitions. There is a calculated red shift of this MLCT of 84 nm in going from bidentate to tridentate coordination of TPYOH in accordance with the experimentally observed respective shifts of 89 and 77 nm, respectively for the A→ B transformations of complex **2** in ethanol and of complex **1** in ethanol-water.

In order to better characterize the photolysis product(s), a DMSO-d_6 solution of complex **2** (~4 mM) was continuously irradiated at 451 nm (3.8 mW) in an NMR tube with a stir bar for 5, 15 and 25 min, and the respective temporal ^{1}H NMR spectra were recorded (Fig. 6). These spectra demonstrate the progressive disappearance of **2** and the appearance of new aromatic resonances in the evolving photolysis solution. At intermediate photolysis

times, a new species appears with aromatic resonances at 8.92, 8.77, 8.72, 8.12, 7.84, 7.49 and 6.94 ppm and a more symmetrical spectrum suggesting the formation of a tricoordinate TPYOH complex. However, these eventually fade with the appearance of a new species with proton resonances very close to those of free TPYOH. Since the conditions (solvent and concentration) of this photolysis experiment were considerably different from those described for Figure 3, samples of these solutions were diluted in water and the optical spectra recorded. Notably, the intermediate photolysis time (15 min) sample displayed increased absorbance between 500 and 550 nm (Figure 6), consistent with formation of intermediate **B**.

Longer term photolysis (2 h) of an analogous solution of **2** resulted in the merging of the resonances representing the aromatic protons of the two symmetrical photolysis product(s) into a "simpler' spectrum with broad peaks at chemical shifts close to those of TPYOH (SI Fig. S13). Photolysis of a DMSO-d_6 solution of complex **1** with sunlight showed a similar trend (SI Fig. S14).

One possible structure for the photolysis product **C** would be a tridentate TPYOH coordinated to Mn(II). To investigate this possibility, the analogous complex, $Mn(TPYOH)Cl_2$ (**3**), was synthesized and structurally characterized. The X-ray crystal structure showed the Mn(II) center to be 5-coordinate in a distorted triangular bipyramid (SI Fig. S15, Table S1, S2). The ^{1}H NMR spectrum of $Mn(TPYOH)Cl_2$ in DMSO-d_6 shows six broad peaks for aromatic protons as does the final photolysis product from complex **1** (SI Fig. S16). The normalized UV-vis spectra in aerobic ethanol of **3** and of **C** are also very similar with a strong absorption band λ_{max} at 408 nm (SI Fig. S16). This absorption for **C** is stable to long term photolysis and is quite different from that of free TPYOH (Table 1). So, it appears that long term photolysis of **1** and **2** leads to a species very similar or identical to that formed when **3** is dissolved in aerobic DMSO and ethanol, respectively. Thus, while a mixture of species might be anticipated given the expected lability of Mn(II), the principal one present is apparently a Mn(II)-TPYOH complex.

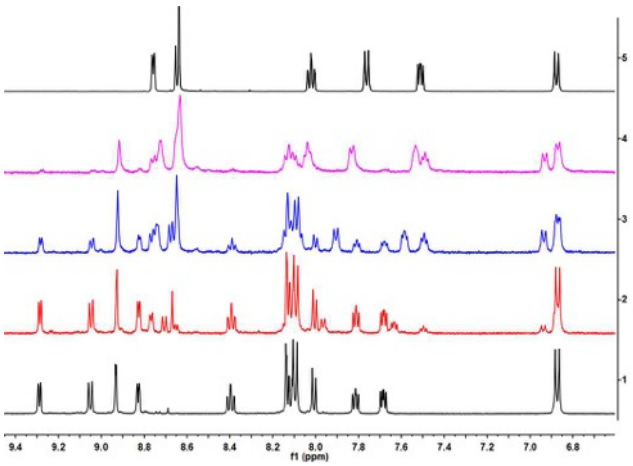

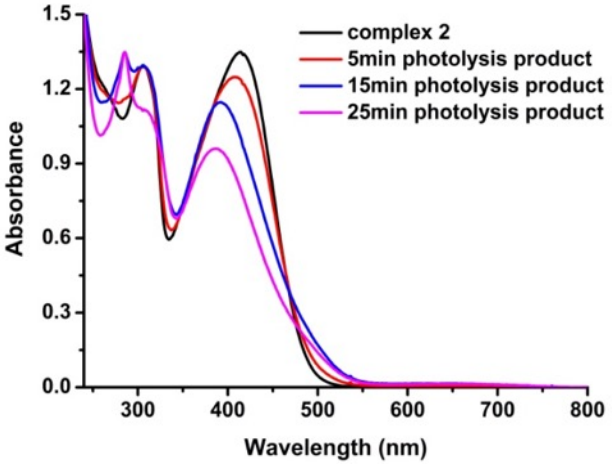

Figure 6. *Top:* Aromatic region of ^{1}H NMR spectra of complex 2 (~4 mM) upon continuous 451 nm (3.8 mW) photolysis in DMSO-d_6 solution. Line 1 is the spectra of complex 2, lines 2, 3 and 4 are spectra of the product after 5, 15 and 25 min photolysis, respectively. Line 5 is the spectrum of TPYOH. *Bottom*: UV-vis spectra of the above solutions after dilution into water (70.2 μM).

Notably, when we isolated and recrystallized the manganese containing bis(TPYOH) complex $[Mn(TPYOH)_2](CF_3SO_3)_2$ (**D**) from the photolysis product solution of **2** in aerobic ethanol. The X-ray crystal structure is shown in SI Figure S17 and experimental details for the crystal structure of **D** are summarized in Table S1. Selected bond lengths and angles are presented in Table S2. The {N,N,N} coordination planes of the two tridentate TPYOH ligands are nearly perpendicular to each other with a dihedral angle of 85.5°. The Mn-N bond lengths are ~0.2 Å longer than those found in η^3-terpyridine Mn(I) complexes but close to those found for **3** and Mn(II) η^3-tris(1-pyrazolyl)methane complexes.[36,37]

Thus, the first stage photoreaction for solutions of complex **2** in DMSO, ethanol or water involves the labilization of one CO to give primarily a dicarbonyl complex, apparently the tricoordinate TPYOH complex $Mn(CO)_2(\eta^3$-TPYOH)X. The photochemical second stage, which is accelerated in aerobic media also results in CO release and, eventually, the formation of Mn(II)-TPYOH complexes (Scheme 3).

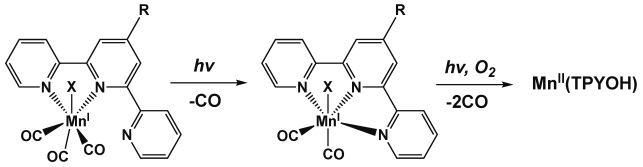

Scheme 3. Proposed photoreaction pathway for the Mn(I) complex **2**. The second structure in the sequence would be species **B**, while the third would be the eventual product in the reaction solution, namely species **C**. (R is *N,N*-bis(2-hydroxyethyl)benzyl, X is triflate or solvent).

The temporal absorbance changes at the MLCT λ_{max} (435 nm) upon photolysis were used to determine the quantum yields ($\Phi_{(A\rightarrow B)}$) for disappearance of complex **2** in the first stage, as calculated from slopes of $N_{reacted}$ versus N_{abs} plots (SI Fig. S18). The values of $\Phi_{(A\rightarrow B)}$ thus de-

termined are 0.26±0.01 in aerobic ethanol and 0.24±0.01 in anaerobic ethanol (three independent measurements, SI Table S5) under 451 nm irradiation. Thus, the effect of oxygen on the photochemical **2→B** process is at most minor.

As noted above (Fig. 4), continued 451 nm irradiation after completion of the first stage leads to a decrease of the 524 nm absorbance, and rates of the second stage (**B→C**) are enhanced by the presence of oxygen. Quantum yields for disappearance of **B** ($\Phi_{B\rightarrow C}$) were determined from temporal absorbance changes at 524 nm as 0.054 ± 0.003 and 0.044 ± 0.005 in aerobic and anaerobic ethanol, respectively (SI Table S5).

The photoreactions of complexes **1** and **2** were also briefly investigated in an aerobic ethanol-phosphate buffer saline (v:v 2:1) The two-stage photoreaction behavior upon 451 irradiation was again observed in both cases. For **2**, the quantum yields $\Phi_{(A\rightarrow B)}$ (0.22 ± 0.01) and $\Phi_{(B\rightarrow C)}$ (0.057 ± 0.001) were essentially the same as observed in neat ethanol (SI Table S6). For **1**, the respective values were 0.19 ± 0.01 and 0.043 ± 0.001.It is notable that the product spectra after the second stage were essentially the same as that of free TPYOH (SI Figs. S19 & S20) in each case. One can rationalize this observation by recognizing that Mn(II) complexes should be relatively labile and that Mn(II) phosphate salts are quite insoluble.[38] Thus, the phosphate would likely strip the manganese from complexes such as **3** or **D**, leaving TPYOH as the only strongly absorbing chromophore in solution.

The photochemistry of complex **2** (~40 μM in aqueous solution) was also examined with a continuous 405 nm LED light source operating at 3.25 mW. The observed two-stage changes in the optical spectra (SI Fig. S21) were analogous to those seen with 451 nm excitation (Fig. 3) with a new absorbance appearing as a shoulder at ~480 nm that then decreases at longer irradiation time. There was little difference in the spectra changes between deaerated and aerobic solutions. SI Figure S21 also shows the spectral changes upon 405 nm photolysis of deaerated aqueous **2** at lower excitation intensity (0.44 mW and 0.23 mW). Under these conditions, the spectral changes primarily reflect the **2→B** first stage. In this case, the photoreaction rate would be proportional to the initial slope of a (ΔA vs irradiation time plot ($\Delta A = A_t - A_0$ at 415 nm). The ratio of the slopes measured for these two excitation intensities is 1.93 which closely matches the 1.91 intensity ratio. This linear response is consistent with this photoreaction being initiated by a single photon excitation process.

Since a 2008 report by Schatzschneider et al,[39] various studies have used the $LMn^{I}(CO)_3$ motif in designing photoCORMs active under excitation by visible or ultraviolet light.[2,11,40-42] The results of the single photon, visible light excitation of **1** and **2**, described in detail here, are qualitatively consistent; namely, CO is labilized with moderate quantum yields upon exciting the dominant MLCT absorption bands. Such systems provide the opportunity to deliver CO precisely to physiological targets but are limited by the low penetration depths of these shorter wavelengths.

Two photon uncaging of CO

The above experiments provide insight into the photoactivity of complex **2** under single-photon excitation, but our primary interest in this compound is focused on its potential sensitivity to simultaneous two-photon excitation. In this regard, an aerobic ethanol solution of **2** (41.1 μM) was subjected to irradiation at 800 nm with ultrafast laser with 100 fs pulses (~60 kW average power during each pulse) at a repetition rate of 80 MHz. While this solution showed minimal spectral changes in the dark, excitation at 800 nm (700 mW overall power) for the same time period led to the optical spectral changes shown in SI Figure S22. Excitation at 750 nm (600 mW) gave similar changes (SI Fig. S23). In both cases there was a progressive decrease in the absorbance at the MLCT band maximum at 435 nm and a blue-shift of the λ_{max}. Figure 7 follows the temporal absorbance decreases at 435 nm for aerobic ethanol solutions of **2** under 750 nm and 800 nm excitation over a period of 140 min with the respective values being 23% and 19%. The expected absorbance change depends on the products formed. Transformation of **2** to **B** would lead to 25% decrease in the absorbance at 435 nm, while **2→C** would give a 43% change, so the observed absorbance changes represent ~50% or more disappearance of **2**.

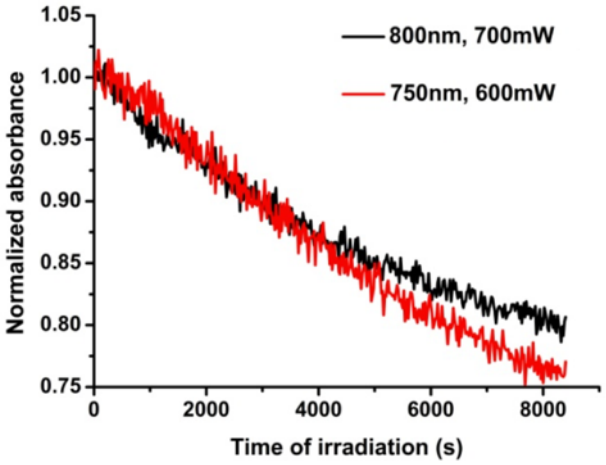

Figure 7. Red line: Temporal absorbance changes at 435 nm upon ultrafast pulsed laser photolysis of **2** (41.1 μM in aerobic ethanol) at 750 nm (600 mW). Black line: Analogous photolysis of **2** (40.5 μM in aerobic ethanol) at 800 nm (700 mW). Data points were recorded at 20 s intervals.

In order to verify the multiphoton character of the process observed in Figure 7, the Ti:Sapphire laser was switched to continuous wave operation at 800 nm. The laser power and beam geometry remained the same as in the mode-locked regime, but under continuous mode the peak power equals the average power (~700 mW). No absorbance decreases were observed with analogous samples under continuous mode photolysis by the NIR laser. Since the laser is delivering the same amount of energy in both modes, the absence of any reaction under continuous clearly demonstrates that the observed reaction cannot be attributed either to single photon excitation at that wavelength or to thermal activation. Thus, the observed photoreaction is clearly the result of a non-linear optical process, namely TPE.

In an analogous experiment an aerobic ethanol solution of **2** (41.3 μM) was irradiated at 800 nm (700 mW) for 60 min (SI Fig. S24) over which time the absorbance decrease at 435 nm was 11.8 %. After the laser was turned off, the decrease in the dark over the next 60 min was 1.8%, suggesting modest thermal reactivity of the photoproduct(s) under these conditions. The absence of a new band in 500-600 nm characteristic of species **B** resulting from the TPE photolysis might suggest that the reaction sequence under these conditions is different than that seen under single photon excitation. This is certainly a possibility given that the selection rules for simultaneous TPE differ from those for SPE. However, given that species **B** undergoes a slow thermal reaction in aerobic media, a more likely explanation is that **B** is being depleted by the latter process over the longer time frame of the NIR excitation experiments.

For a process triggered by TPE, the parameter measured (photoluminescence intensity, photolysis rate, etc.) is expected to be a nonlinear function of the excitation intensity.[29] In order to address this question, experiments to measure the photolysis process as a function of irradiation intensity were undertaken. The experimental setup was similar to that described above with neutral density filters used to attenuate the 800 nm laser. Irradiation power(s) were measured using a thermopile optical power meter**.** Solutions of **2** (~39 μM in aerobic ethanol and ~34 μM in anaerobic ethanol) were irradiated at different laser powers for a certain time period, and the absorbance changes were recorded (SI Figs. S25 & S26). The largest differential absorbances (A_t-A_0) were found at 450 nm, and plots of A_t-A_0 at 450 nm vs irradiation time are shown in Figure 8. The relative rates R of the NIR photochemically induced absorbance changes were then calculated from the initial slopes of (A_t-A_0)/A_0 vs irradiation time plots for 800 nm photolysis of **2** at different laser powers**.** Plots of log (R) versus log (power) are shown in Figure 9. The slope of each is ~1.6. Thus, the NIR-initiated photoreactions are clearly nonlinear functions of excitation intensity; however, the slopes of these plots are less than the values of ~2 that might be expected for a simple TPE induced process.[29]

Carbon monoxide release resulting from such NIR excitation was determined as described above using the GC-TCD analysis of the gas phase above the photolysis solutions contained in Schlenk cuvettes. TPE photolysis at 800 nm of **2** in aerobic ethanol clearly led to CO release. The stoichiometry of this process is somewhat ambiguous, since the spectral changes displayed in SI Figures S22-S26 likely reflect a combination of photoinduced **2** → **B** and

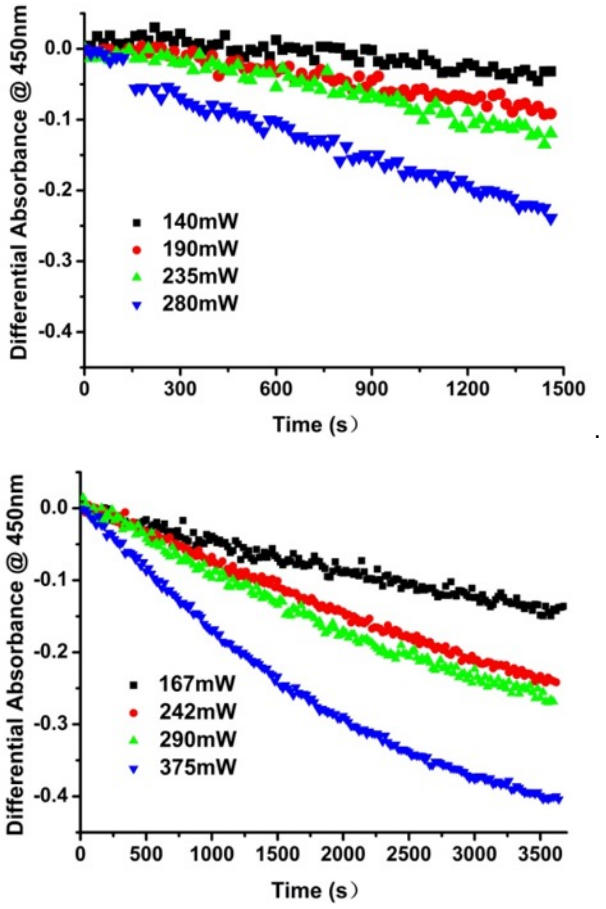

Figure 8. *Top:* Temporal absorbance differences (A_t-A_0) measured at 450 nm for the 800 nm laser photolysis of 2 (~39 μM) in aerobic ethanol at different excitation powers (140, 190, 235 OR 280 MW). *Bottom:* Temporal absorbance differences (A_t-A_0) measured at 450 nm for the 800 nm laser photolysis of **2** (~34 μM) in anaerobic ethanol at different excitation powers (167, 242, 290 or 375 mW). Data were recorded at 20 s intervals.

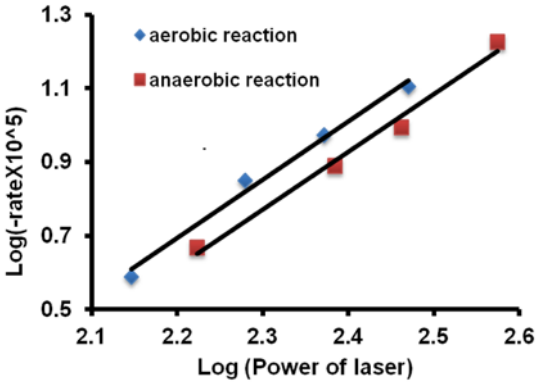

Figure 9 log(-rate x10^{-5}) versus log (power of the laser) plots upon 800 nm photolysis of **2** (41 μM) at different laser powers in aerobic and anaerobic ethanol. The slopes are, respectively, 1.58 and 1.56. Conditions and concentrations are those reported in Figure 8.

B → **C** reactions as well as some thermal reactivity of the intermediate **B** in the aerobic media. However, the differ-

ence spectra displayed more closely resemble that for the **2** → **C** transformation shown in Figure 3. SI Table S7 summarizes experiments where the CO was measured by GC-TCD and the final absorbance at 435 nm was used to determine the % reaction, assuming that the process observed spectrally was **2** → **C**. On this basis, the ratio of the moles of CO released to the moles of **2** depleted by NIR excitation is ~two or somewhat larger. The uncertainty can also be attributed in part to the relatively small GC-TCD signals for CO that occur on the shoulder of the much stronger signal for the N_2 present in the aerated solutions.

SUMMARY

In brief, we have reported the synthesis and characterization of aqueous-soluble photoCORMs derived from the two photon chromophore 4'-p-N,N-bis(2-hydroxyethyl) benzyl-2,2':6',2''-terpyridine (TPYOH). These complexes release CO under single-photon excitation with visible light and, more notably under two-photon excitation with NIR light. For the SPE photolysis, a two-stage photochemical process was found to be induced by visible light; one CO was released during the first stage and approximately two more CO's were released during the second stage. This structural motif is shown to be photoactive when subjected to high intensity pulsed laser photolysis at 750 nm or 800 nm lasers leading to CO release. The non-linear response (log(rate) vs log(power) plot) of the NIR activated photochemical reactions of **2** to varied laser power indicates that it responds to multiphoton excitation under these conditions. However, the slow photoreaction rates suggest that the two photon cross sections of **2** is smaller than anticipated. While this study provides a valuable proof-of-principle example of photoCORM activation by two photon excitation with tissue transmitting near-infrared light, practical application of NIR TPE under physiological conditions will require chromophores with stronger cross sections. Ongoing studies in these laboratories will address these issues.

EXPERIMENTAL SECTION

Materials

$Mn(CO)_5Br$ and silver triflate were purchased from Strem Chemicals. All commercially available reagents were used as purchased without further purification.

Analytical instruments

Solution optical absorption spectra were recorded in 1.0 cm pathlength quartz cells using Shimadzu dual beam UV-2401 PC and StellarNet SL5-DH spectrophotometers. Infrared spectra of solutions were measured in cells with CaF_2 windows using a Mattson Research Series FTIR spectrometer. Solid state IR spectra were obtained using a Perkin Elmer Spectrum Two UATR FT-IR Spectrometer. Solution NMR spectra were recorded using a Varian Unity Inova 500 MHz spectrometer. Exact molecular masses were measured using a Waters (Milford, MA) GCT Premier time-of-flight mass spectrometer with electrospray (ES) ion sources. CO release was quantified using an Agilent 6890 gas chromatograph with a thermal conductivity detector (GC-TCD).

X-ray crystallography

The solid-state crystal structures were determined by X-ray diffraction on a Kappa Apex II single-crystal diffractometer. The X-ray structural data are summarized in the Table S1. The structure of *fac*-$[Mn(CO)_3(TPYOH)Br]$ was refined using SHELXL-2014/7 while the structures of $Mn(TYPOH)Cl_2$ and $Mn^{II}(TPYOH)_2(CF_3SO_3)_2$ were refined using SHELXL-2018/1 (see cif files).

Syntheses

4'-p-N,N-bis(2-hydroxyethyl)benzyl-2,2':6',2''-terpyridine: TPYOH was prepared by a published procedure.[31,32] ^{1}H NMR (d_6-DMSO, 500 MHz): 8.76(d, 2H, J = 5.0, H_g), 8.65(2H, d, J = 5.0, H_d), 8.64(2H, s, H_c), 8.02 (2H, td, J=8.0, 1.5H_e), 7.77(2H, d, J = 9.0, H_b), 7.51 (2H, td, J = 8.0, 1.5, H_f), 6.88 (2H, d, J = 9.0, H_a), 4.82 (2H, t, -OH), 3.60 (4H, t, J = 6.0, -NCH_2-), 3.51(4H, t, J=6.0, -CH_2O-).

*fac-[Mn(CO)$_3$(TPYOH)Br] (**1**)*: Bromidopentacarbonylmanganese(I), $Mn(CO)_5Br$ (95 mg, 0.35 mmol) and TPYOH (108 mg, 0.26 mmol) were dissolved in acetone (30 mL). The solution was heated at reflux for 3 h under argon atmosphere. The resulting yellow suspension was cooled to room temperature resulting in a yellow precipitate. The solid was collected by filtering and washed by diethyl ether. The crude product was dissolved in small amount of dimethylformamide and then loaded on an alumina chromatography column and eluted with ethyl acetate /methanol (1:1, v:v). The orange-red fraction was collected and the solvent was removed to obtain a yellow powder that was dried in vacuum. Single crystals, suitable for X-ray diffraction analysis, were obtained by slow diffusion of diethyl ether into an acetone solution of complex **1**. Yield: 136 mg (83 %). ^{1}H NMR (d_6-DMSO, 500 MHz): 9.19 (d, 1H, J = 5.0, H_i), 8.96 (1H, d, J = 8.0, H_l), 8.84 (1H, s, H_h), 8.79 (1H, d, J = 4.0, H_g), 8.27(1H, t, J = 8.0, 10, H_j), 8.06 (1H, t, J = 8.0, H_e), 8.04 (2H, d, J = 8.5, H_b), 7.98 (1H, s, H_c), 7.95 (1H, d, J = 8.0, H_d), 7.70 (1H, t, J = 6.0, H_k), 7.61 (1H, m, J = 5.0, 7.0, H_f), 6.87 (2H, d, H_a, J = 8.5, H_a), 4.82 (2H, t, -OH), 3.60 (4H, t, J=6.0, -NCH_2-), 3.53(4H, t, J=6.0, -CH_2O-). FTIR (C≡O stretching region): $\tilde{\nu}$ = 2017 (s), 1937(s) and 1885(s) cm^{-1}. Elemental Analysis for $C_{28}H_{24}BrMnN_4O_5.H_2O$: Calc'd: C, 51.79; H, 4.04, N, 8.63. Found: C, 51.61; H, 4.02; N, 8.56. ESI-MS (m/z) $[Mn(CO)_3(TPYOH)]^+$: 551.1; $[Mn(CO)_3(TPYOH)(CH_3CN)]^+$: 592.2.

*fac-[Mn(CO)$_3$(TYPOH)(CF$_3$SO$_3$)] (**2**):* A sample of **1** (32 mg, 0.05 mmol) was dissolved in acetone (30 mL) in the dark. $Ag(CF_3SO_3)$ (20 mg, 0.08 mmol) was then added to the mixture. After stirring for 30 min at room temp., the AgBr precipitate was removed by centrifugation. The solution was then evaporated under reduced pressure to obtain a 1 mL concentrated solution, which was dropped into 10 mL diethyl ether to give a red precipitate. The precipitate was collected by centrifugation and rinsed with diethyl ether (2 × 10 mL) before being dried overnight in a desiccator under vacuum. Yield : 32 mg (90 %). ^{1}H NMR (d_6-DMSO, 500 MHz): δ H(ppm): 9.29 (1H, d, J=5.5, H_i), 9.06 (1H, d, J=8.5, H_l), 8.93(1H, s, H_h), 8.83 (1H, d, J=5.0, H_g), 8.40 (1H, td, J=8.0, 1.5, H_j), 8.14 (1H, s, H_c), 8.12(1H, td, J=8.0, 1.5, H_e), 8.10 (2H, d, J=9.0, H_b), 8.01 (1H, d, J=8.0, H_d), 7.82 (1H, td, J=7.0, 1.0, H_k), 7.68 (1H, td, J=7.0, 1.0, H_f), 6.88(2H, d, J=9.0, H_a), 4.84 (2H, t, -OH), 3.60 (4H, t, J=5.5, -NCH_2-), 3.55 (4H, t, J=5.5, -CH_2O-). FTIR (C≡O stretching region): $\tilde{\nu}$ = 2033 (s), 1923(s) cm^{-1}. Elemental Analysis for $C_{29}H_{24}F_3MnN_4O_8S$ Calc'd: C, 49.72; H, 3.45; N, 8.00. Found: C, 50.68, H, 3.65, N, 8.42. ESI-MS (m/z) $[Mn(CO)_3(TPYOH)]^+$: 551.1; $[Mn(CO)_3(TPYOH)(CH_3CN)]^+$: 592.1.

*$Mn(TYPOH)Cl_2$ (**3**)*: TPYOH (90 mg, 0.20 mmol) and $MnCl_2$•$4H_2O$ (19.9 mg, 0.10 mmol) were dissolved in methanol (25 mL) and the solution was heated at reflux overnight. After that the red suspension was cooled to room temperature resulting in a red precipitate. The solid was collected by filtering and washed with diethyl ether. The latter was recrystallized from methanol. Single crystals suitable for X-ray diffraction analysis were obtained by slow diffusion of acetone into a methanolic solution of **3.** During the refinement of the structure for **3**, the residual peaks of solvents could not be identified, and were removed by using the SQUEEZE routine of PLATON. Besides, DFIX, ISOR, SIMU and EADP were used to restrain the disorder of O5, O5', C63, C63', C64, and C64' to realize a more acceptable molecular model and to avoid the ADP mistakes. ISOR was used to restrain the anisotropy U values of Cl3 and O4 for ADP problems. The X-ray structure as well as the FTIR and optical spectra are shown in SI Figures S15 and S16.

Photochemical Studies

SPE photolysis procedures. Photolysis experiments were carried out using 405 and 451 nm light emitting diodes (LUXEON Rebel) operating at room temperature (Fig. S7). Light source power was measured with a PM100USB power meter. The solutions were contained in a custom-made Schlenk cuvette consisting of a 1.0 cm pathlength cuvette fused to glass tubing and stopcocks designed for attaching to a vacuum line for degassing or introducing a specific gas.[10] This apparatus has a port sealed by a septum, through which gas samples are withdrawn for GC−TCD analysis. Solutions for anaerobic experiments were degassed by freeze−pump−thaw procedures (3X), after which the Schlenk cuvette was backfilled with purified argon. After photolysis, the gas phase was sampled by drawing an aliquot with a gas-tight syringe and analyzing it by GC−TCD. The total CO released during photolysis was then calculated by accounting for the cell volume, solution volume, CO solubility in the solvent and the partitioning of CO between the gas and liquid phases.

Quantum yield measurements used the power meter to measure the LED power incident on the solution at the irradiation wavelength λ_{irr}. Photons absorbed (N_{abs}) were calculated from the incident photon flux (I_0) and the solution absorbance (Abs) at λ_{irr} according to eqs. 1 and 2.

$$I_0 = P/E \quad (1)$$

$$N_{abs} = (1\text{-}10^{-Abs}) \times I_0 x\, t \quad (2)$$

where P = power in J/s, E = J photon^{-1} at λ_{irr}, and t = photolysis time in s.[20]

The number of molecules reacted ($N_{reacted}$) can be calculated from the absorption changes (Abs_0-Abs_t) at monitoring wavelengths where extinction coefficient changes ($\Delta\varepsilon = \varepsilon_0 - \varepsilon_{final}$) and the solution volume are known. The quantum yield Φ can thus be determined from eq. 3. In practice, Φ values were not determined from single data points but from the slopes of the $N_{reacted}$ versus N_{abs} plots (eqs. 3) as shown in SI Figure S18.[20]

$$\Phi = N_{reacted} / N_{abs} \quad (3)$$

TPE photolysis procedures: TPE photochemical measurements were carried out with the UCSB Optical Characterization Facility. The photolysis apparatus used in this facility is diagramed and described in SI Figure S27. Two different laser systems were used. In the initial experiments (Fig. 8), samples were excited with a tightly collimated (diameter ~120 μm) high-intensity laser beam. TPE at 750 nm and 800 nm was achieved using a mode-locked Ti:sapphire laser (Spectra Physics Tsunami) with excitation pulses of ~100 fs and energy of ~6 nJ operating with a repetition rate of 80 MHz. Power dependence studies (Figs. 8 & 9 plus SI Figs. S24 & S25) utilized an Astrella Ti:Sapphire laser system with excitation pulses ~110 fs operating at 5 kHz repetition rate with a beam diameter about 3 mm, thereby giving significantly higher pulse peak intensities. Incident photon flux during photolysis was measured using Newport optical power/energy meter model 8442 PE with a silicon photodiode model 884 UVR detector.

DFT calculations

DFT calculations were performed with Spartan'14 software packages at a B3LYP/6-31G* level of theory. Optimized ground state structures of complex **1** ($Mn(\eta^2\text{-}TPYOH)(CO)_3Br$) and of $Mn(\eta^3\text{-}TPYOH)(CO)_2Br$ (in vacuum) were used.

ASSOCIATED CONTENT

Supporting Information

Crystallographic data was deposited at the Cambridge Crystallographic Data Centre under CCDC-1811760 for $[Mn(CO)_3(TPYOH)Br]$, CCDC-1860554 for $Mn(TPYOH)Cl_2$ and CCDC-1882575 for $Mn(TPYOH)(CF_3SO_3)_2$, This data is obtained free of charge via www.ccdc.cam.ac.uk/conts/retrieving.html (or from the Cambridge Crystallographic Data Centre, 12, Union Road, Cambridge CB2 1EZ, UK; fax: (+44) 1223-336-033; or deposit@ccdc.cam.ac.uk).

Other Supporting Information is available free of charge on the ACS Publications website at DOI:

Additional documentation (7 tables and 27 figures of the studies described in the manuscript (PDF).

AUTHOR INFORMATION

Corresponding Authors

* Q.J. E-mail: jq6898741@163.com

* P.S. E-mail: shipfoo9@163.com

* P.C.F. E-mail: ford@chem.ucsb.edu

ORCID

Peter C. Ford: 0000-0002-5509-9912

Notes

The authors declare no competing financial interest

Author Contributions

The manuscript was written through contributions of all authors. All authors have given approval to the final version of the manuscript.

Funding Sources

(This work was supported by grants to P.C.F. from the Chemistry Division of the United States National Science Foundation (Grants CHE-1405062 and CHE-

1565702). The Coherent Astrella ultrafast laser system was funded by DURIP ARO grant 66886LSRIP

ACKNOWLEDGMENTS

Q.J. was supported by the Overseas Research & Training Program for University Prominent Young & Middle-aged Teachers and Presidents and by the Key Science and Technology Project from Lianyungang city (CG1517 and JC1608). We thank Dr. Zhi Li for his advice on photolysis techniques.

REFERENCES

1 Motterlini, R.; Otterbein, L. The therapeutic potential of carbon monoxide. *Nat. Rev. Drug Discovery*, **2010**, *9*, 728−743.

2 Schatzschneider, U. Novel lead structures and activation mechanisms for CO-releasing molecules (CORMs). *Brit. J. Pharmacol.*, **2015**, *172*, 1638–1650.

3 Heinemann, S. H.; Hoshi, T.; Westerhausen, M.; Schiller, A. Carbon monoxide – physiology, detection and controlled release. *Chem. Commun*., **2014**, *50*, 3644−3660.

4 García-Gallego, S.; Bernardes, G. J. L. Carbon-Monoxide-Releasing Molecules for the Delivery of Therapeutic CO In Vivo, *Angew. Chem. Int. Ed.* **2014**, *53*, 9712-9721.

5 Babu, D.; Motterlini,R.; Lefebvre, R. A. CO and CO-releasing molecules (CO-RMs) in acute gastrointestinal inflammation**.** *Br. J. Pharmacol.* **2015**, *172,* 1557−1573.

6 Kitagishi, H.; Minegishi, S.; Yumura, A.; Negi, S.; Taketani, S.; Amagase, Y.; Mizukawa, Y.; Urushidani, T.; Sugiura, Y.; Kano, K.Feedback Response to Selective Depletion of Endogenous Carbon Monoxide in the Blood. *J. Am. Chem. Soc.*, **2016**, *138*, 5417−5425.

7 Nobre, L. S.; Jeremias, H.; Romão, C. C.; Saraiva, L. M. Examining the antimicrobial activity and toxicity to animal cells of different types of CO-releasing molecules. *Dalton Trans.*, **2016**, *45*, 1455−1466.

8 Wareham, L. K.; Poole, R. K.; Tinajero-Trejo, M. CO-releasing Metal Carbonyl Compounds as Antimicrobial Agents in the Post-antibiotic Era. *J. Biol. Chem*. **2015**, *290*, 18999-19007.

9 Romão, C. C.; Blättler, W. A.; Seixas, J. D.; Bernardes, G. J. L Developing drug molecules for therapy with carbon monoxide. *Chem. Soc. Rev.*, 2012, 41, 3571–3583.

10 Rimmer, R. D.; Richter, H.; Ford P C. A Photochemical Precursor for Carbon Monoxide Release in Aerated Aqueous Solution. *Inorg. Chem*. **2010***, 49*, 1180-1185.

11 Ford, P. C. Metal complex strategies for photo-uncaging the small molecule bioregulators nitric oxide and carbon monoxide, *Coord. Chem. Rev.* **2018**, *376*, 548-564.

12 Marker, S. C.; MacMillan S. M.; Zipfel, W. R.; Li, Z.; Ford, P. C.; Wilson, J. J Photoactivated *in Vitro* Anticancer Activity of Rhenium(I) Tricarbonyl Complexes Bearing Water-Soluble Phosphines. *Inorg. Chem*. **2018**, *57*, 1311-1331.

13 Soboleva,T.; Esquer, H. J.; Anderson, S. N.; Berreau, L. M.; Benninghoff, A. D. Mitochondrial-Localized Versus Cytosolic Intracellular CO-Releasing Organic PhotoCORMs: Evaluation of CO Effects Using Bioenergetics *ACS Chem. Biol.* **2018,** *138,* 2220-2228.

14 Inaba, H.; Fujitab, K.; Ueno, T.Design of biomaterials for intracellular delivery of carbon monoxide *Biomater. Sci.*, **2015**, *3*, 1423–1438.

15 Rimmer, R. D.; Pierri, A. E.; Ford P. C. Photochemically Activated Carbon Monoxide Release for Biological Targets. Developing Air-Stable Group 6 PhotoCORMs Labilized by Visible Light. *Coord. Chem. Rev.*, **2012**, *256*, 1509-1519.

16 Marhenke, J.; Trevino, K.; Works C. F. The chemistry, biology and design of photochemical CO releasing molecules and the efforts to detect CO for biological applications. *Coord. Chem. Rev.*, **2016**, *306*, 533–543.

17 Chakraborty, I.; Carrington, S. J.; Mascharak, P. K.; Design Strategies to Improve the Sensitivity of Photoactive Metal Carbonyl Complexes (photoCORMs) to Visible Light and Their Potential as CO-Donors to Biological Targets. *Acc. Chem. Res.,* **2014**, *47*, 2603−2611.

18 Kottelat, E.; Ruggi, A.; Zobi, F. Red-light activated photo-CORMs of Mn(I) species bearing electron deficient 2,2′-azopyridines. *Dalton Trans*. 2016, **45**, 6920−6927.

19 Askes, S. H. C.; Reddy, G.; Upendar ,W.; Bonnet, S.; Schiller, A. Red Light-Triggered CO Release from $Mn_2(CO)_{10}$ Using Triplet Sensitization in Polymer Nonwoven Fabrics *J. Am. Chem. Soc*. **2017**, *139*, 15292-15295.

20 Li, Z.; Pierri, A. E.; Huang, P.-J.; Wu, G.; Iretskii, A. V.; Ford, P. C., Dinuclear PhotoCORMs: Dioxygen-Assisted Carbon Monoxide Uncaging from Long-Wavelength -Absorbing Metal-Metal-Bonded Carbonyl Complexes. *Inorg. Chem.*, **2017**, *56*, 6094−6104.

21 Smith, A. M.; Mancini, M. C.; Nie, S. Bioimaging. Second window for *in vivo* imaging. *Nature Nanotech*. **2009**, *4*, 710-711.

22 Nikolenko, V.; Yuste, R.; Zayat, L.; Baraldo, L. M.; Etchenique R. Two photon uncaging of neurochemicals using inorganic metal complexes, *Chem. Commun.* **2005**, *41,* 1752-1754

23 Ford, P. C., Polychromophoric Metal Complexes for Generating the Bioregulatory Agent Nitric Oxide by Single and Two Photon Excitation, *Acc. Chem. Res*. **2008**, *41*, 190-200.

24 Burks, P. T.; Garcia, J. V.; GonzalezIrias, R.; Tillman, J. T. ; Niu, M. Zhang, J.P.; Zhang, F. Ford, P. C. Nitric Oxide Releasing Materials Triggered by Near-Infrared Excitation Through Tissue Filters,J. Am. Chem. Soc. 2013, 135, 18145-18252.

25 Garcia, J. V.; Yang, J.; Shen, D.; Yao, C.; Li, X.; Wang, R.; Stucky, G. D.; Zhao, D.; Ford, P. C.; Zhang, F. NIR-Triggered Release of Caged Nitric Oxide Using Upconverting Nanostructured Materials. *Small* **2012**, *8*, 3800–3805.

26 Pierri, A. E.; Huang, P.-J.; Garcia, J. V.; Stanfill, J. G.; Chui, M.; Wu, G.; Zheng N. F.; Ford, P. C. PhotoCORM nanocarrier for CO release using NIR light. *Chem. Commun.*, **2015**, *51*, 2072–2075.

27 Ou, J.; Zheng, W.; Xiao, Z, Y.; Yan, X. P.; Jiang, X. J.; Dou, Y.; Jiang R.; Liu, X. M. Core-shell materials bearing iron(II) carbonyl units and their CO-release via an upconversion process. *J. Mater. Chem. B* **2017**, *5*. 8161-8168.

28 Wecksler, S. R.; Mikhailovsky, A.; Korystov, D.; Buller, F.; Kannan, R.; Tan, L.-S.; Ford, P. C. Single and two photon properties of a dye derivatized Roussin's red salt ester ($Fe_2(\mu\text{-}RS)_2(NO)_4$) with a large TPA cross section, *Inorg. Chem.* **2007**, *46*, 395-402.

29 Wecksler, S. R.; Mikhailovsky A.; Korystov D.; Ford, P. C. A Two-Photon Antenna for Photochemical Delivery of Nitric Oxide from a Water Soluble, Dye Derivatized Iron Nitrosyl Complex Using NIR Light. *J. Am. Chem. Soc.*, **2006**, *128*, 3831-3837.

30 Zheng Q.; Bonoiu, A.; Ohulchansky, T. Y.; He G. S.; Prasad, P. N. Water-Soluble Two-Photon Absorbing Nitrosyl Complex for Light Activated Therapy Through Nitric Oxide Release. *Mol. Pharm*. **2008**, *5,* 389-398.

31 Tan, L.; Wan, A.; Zhu, X.; Li, H. Nitric oxide release triggered by two-photon excited photoluminescence of engineered nanomaterials. *Chem. Commun*. **2014**, *50*, 5725-5728.

32 Thomsen, H.; Marino, N.; Conoci, S.; Sortino, S. Ericson, M. B. Confinedpho to-release of nitric oxide with simultaneous two-photon fluorescence tracking in a cellular system. *Scientific Reports*, **2018**, *8*, Article 9753

33 Shi, P.; Jiang, Q.; Zhao, X.; Zhang, Q.; Tian, Y., Study of the one-photon and two-photon properties of two water-soluble terpyridines and their zinc complexes. *Dalton Trans*., **2015**, *44*, 8041-8048

34 Shi P.; Jiang, Q. China patent No. ZL201210006616.0, 2012.

35 Ramu,V; Reddy, G. U; Liu, J.; Hoffmann, P.; Sollapur, R.; Wyrwa, R.; Kupfer, S.; Spielmann, C.; Bonnet, S.; Neugebauer, U.; Schiller; A. Two-Photon-Induced CO-Releasing Molecules as Molecular Logic Systems in Solution, Polymers, and Cells. Chem. Eur. J. **2019** in press

36 Compain, J.-D.; Stanbury, M.; Trejo, M.; Chardon-Noblat, S. Carbonyl-Terpyridyl-Manganese Complexes: Syntheses, Crystal Structures, and Photo-Activated Carbon Monoxide Release Properties. *Eur. J. Inorg. Chem.* **2015**, 5757–5766.

37 Sachs, U.; Schaper, G., Winkler, D. Kratzert, D. Kurz P., Light- or oxidation-triggered CO release from $[Mn^{I}(CO)_3(k^3\text{-}L)]$ complexes: reaction intermediates and a new synthetic route to $[Mn_2^{III/IV}(\mu\text{-}O)_2(L)_2]$ compounds. *Dalton Trans.*, **2016**, *45*, 17464–17473.

38 Mahapatra, P. P.; Dash, A. K.; Chickerur, N.S. Solubility and Thermodynamic Data of Manganese Hydrogen Phosphate in the System $MnO\text{-}P_2O_5\text{-}H_2O$ at 35, 40, 45 and 50 °C. *Thermochimica Acta*, **1983**, *10*, 163-171.

39 Niesel, J.; Pinto, A.; N'Dongo, H. W. P.; Merz, K.; Ott, I.; Gust, R.; Schatzschneider, U. Photoinduced CO release, cellular uptake and cytotoxicity of a tris(pyrazolyl) methane (tpm) manganese tricarbonyl complex**.** *Chem. Commun*. **2008,** *15*, 1798-1800.

40 Pierri, A. E.; Muizzi, D. A.; Ostrowski, A. D.; Ford, P. C. Photo-Controlled Release of NO and CO with Inorganic and Organometallic Complexes, *Structure & Bonding* **2015**, *165,* 1-45

41 Jimenez, J.; Chakraborty, I.; Dominguez, A.; Martinez-Gonzalez, J.; Sameera, W. M. C.; Mascharak, P. K. A Luminescent Manganese PhotoCORM for CO Delivery to Cellular Targets under the Control of Visible Light. *Inorg. Chem.* **2018**, *57*, 1766-1773.

42 Mansour, A. M., Green-Light-Induced PhotoCORM: Lysozyme Binding Affinity towards Mn-I and Re-I Carbonyl Complexes and Biological Activity Evaluation, *Eur. J. Inorg. Chem*. **2018**, *44*, 4805-4811

TABLE OF CONTENTS FIGURE:

Two photon excitation with NIR light (800 nm) uncages CO from the photoCORM $Mn(CO)_3(TPYOH)X$ (TPYOH = 4'-p-N,N-bis(2-hydroxyethyl)benzyl-2,2':6',2''-terpyridine)